

Adaptive State-of-Charge Estimation Based on a Split Battery Model for Electric Vehicle Applications

Jufeng Yang, *Student Member, IEEE*, Bing Xia, *Student Member, IEEE*, Yunlong Shang^{1b}, *Student Member, IEEE*, Wenxin Huang, *Member, IEEE*, and Chunting Chris Mi^{1b}, *Fellow, IEEE*

Abstract—The conventional state-of-charge (SoC) estimation methods based on the equivalent circuit model (ECM) integrate all state variables into one augmented state vector. However, the correlations between RC voltages and SoC degrade the stability and accuracy of the estimates. To address this problem, this paper presents an adaptive SoC estimation method based on the split battery model, which divides the conventional augmented battery model into two submodels: the RC voltage submodel and the SoC submodel. Hence, the cross interference between RC voltages and SoC is reduced, which effectively reduces the oscillation in the estimation and improves the estimation accuracy. In addition, the adaptive algorithm is applied on the SoC submodel to improve the system robustness to noise disturbances. A case of a second-order ECM is analyzed and two types of Lithium-ion batteries are employed to verify the universality of the proposed method. Experimental results show that the undesired oscillation is eliminated during the convergence stage and the maximum SoC error is within 1% over a wide SoC range.

Index Terms—Adaptive extended Kalman filter (AEKF), electric vehicles (EVs), Lithium-ion batteries, state-of-charge (SoC), split battery model (SBM).

I. INTRODUCTION

LITHIUM-ION batteries are the main choice for energy storage in electric vehicles (EVs) due to the advantages of low self-discharge rate, high energy and high power densities

Manuscript received January 5, 2017; revised June 1, 2017; accepted July 8, 2017. Date of publication July 19, 2017; date of current version December 14, 2017. This work was supported in part by the China Scholarship Council, in part by the US DOE Graduate Automotive Technology Education Center of Excellence, and in part by Nanjing Golden Dragon Bus Company, Ltd. The review of this paper was coordinated by Dr. C. Liu. (*Corresponding author: Chunting Chris Mi.*)

J. Yang is with the Department of Electrical Engineering, Nanjing University of Aeronautics and Astronautics, Nanjing 211106, China, and also with the Department of Electrical and Computer Engineering, San Diego State University, San Diego, CA 92182 USA (e-mail: nuayjf@163.com).

B. Xia is with the Department of Electrical and Computer Engineering, San Diego State University, San Diego, CA 92182 USA, and also with the Department of Electrical and Computer Engineering, University of California San Diego, San Diego, CA 92093 USA (e-mail: bixia@eng.ucsd.edu).

Y. Shang is with the Department of Electrical and Computer Engineering, San Diego State University, San Diego, CA 92182 USA, and also with the School of Control Science and Engineering, Shandong University, Jinan 250061, China (e-mail: shangyunlong@mail.sdu.edu.cn).

W. Huang is with the Department of Electrical Engineering, Nanjing University of Aeronautics and Astronautics, Nanjing 211106, China (e-mail: huangwx@nuaa.edu.cn).

C. C. Mi is with the Department of Electrical and Computer Engineering, San Diego State University, San Diego, CA 92182 USA (e-mail: mi@ieee.org).

Color versions of one or more of the figures in this paper are available online at <http://ieeexplore.ieee.org>.

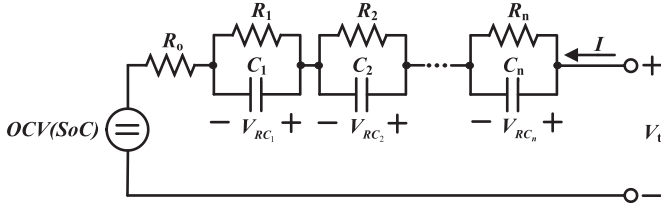
Digital Object Identifier 10.1109/TVT.2017.2728806

[1], [2]. To ensure the safety and reliability of battery systems, a well-designed battery management system (BMS) is of significant importance [3]–[5]. One of the core tasks of the BMS is to provide the accurate state-of-charge (SoC), which is defined as an indicator of the available capacity remaining in the battery compared to the full capacity. Unlike the gas gauge, the SoC cannot be measured directly from physical sensors, and is closely related to the complex electrochemical reactions. Hence, calculating an accurate SoC is still a challenging task.

The existing SoC estimation methods can generally be divided into two categories: open-loop and closed-loop estimation methods.

The Coulomb counting (CC) and the OCV measurement methods are two commonly used open-loop SoC estimation methods. They are straightforward and easy to implement. Nevertheless, the CC method is vulnerable to the noise of the current sensor, and highly depends on the precision of the initial SoC. While for the OCV measurement method, the sufficient rest time is required to ensure the measured battery terminal voltage is close to the OCV value, which is infeasible from a practical point of view [6]. In addition, the estimation result is sensitive to the voltage measurement accuracy. Especially for the battery chemistry with a flat SoC-OCV curve, e.g., LiFePO₄ battery, a slight error on the OCV can induce a large error on the estimated SoC [7].

In contrast, the closed-loop estimation methods can effectively overcome the drawbacks associated with the CC and OCV measurement methods and provide robust SoC estimation. These methods can be classified into two groups, namely, the data-driven based and the equivalent circuit model (ECM) based methods. The data-driven based methods employ techniques such as fuzzy logic [8], artificial neural networks (ANN) [9], [10] and support vector machines (SVM) [11] to train the “black box” model with a large amount of collected testing data. Most of these methods are prohibitive for on-board implementation due to the overload in the computational cost. On the other hand, the electrical behavior of the battery can be described by the ECM, and the associated state variables, including RC voltages and SoC, are estimated online through a variety of model based filters or observers, such as extended Kalman filter (EKF) [12]–[14], particle filter [15], H-infinity filter [16], [17] and sliding mode observer [18], [19]. Among them, the EKF related estimation methods are very promising. Since only basic matrix operations are involved in this type of estimation method, it can be easily conducted on the automotive microcontroller, making

Fig. 1. n th-order ECM.

it valuable in the practical applications. However, the performance of the EKF related estimation methods strongly depends on the predetermined values of the system noise. Lee in [20] proposes a battery model with a measurement noise model and data injection to regulate the measurement noise covariance. Xiong in [21]–[23] employs the covariance matching approach to adaptively update the system noise. Zhang in [24] develops an adaptive SoC estimation framework by integrating the SoC estimation schemes with the identification algorithms. Zhang in [25] utilizes the wavelet transform matrix to de-noise both noisy current and voltage signals, and employs the adaptive extended Kalman filter (AEKF) to adjust the noise covariance. These methods can improve the accuracy and the robustness of the SoC estimation to a certain extent. It has to be noted that in the existing EKF related estimation methods, RC voltages and SoC are usually coupled together to form one augmented state vector. However, the uncertainty on the estimated RC voltage disturbs the estimated SoC and vice versa. Hence, the cross interference between these two types of state variables can degrade the estimation convergence at the start-up stage, and reduce the estimation accuracy at the stable stage.

In this paper, an adaptive SoC estimation method is proposed on the basis of the split battery model (SBM). The SBM is achieved by decoupling the conventional augmented battery model (ABM) into two submodels: the RC voltage submodel and the SoC submodel. Owing to the decoupling, the cross interference terms in the expression of Kalman gain are eliminated, which is beneficial for reducing the oscillation and estimation error. Moreover, the adaptive algorithm is applied on the SoC submodel to improve the system robustness to the process and measurement noise. Experiments are carried out on two types of lithium-ion batteries (the LiFePO₄ battery and the LiNMC battery) to validate the feasibility and robustness of the developed estimation approach. Furthermore, comparison with the conventional estimation method demonstrated the advantages of the proposed method in terms of convergence performance and estimation accuracy.

II. ABM BASED AEKF ESTIMATION METHOD

A. Algorithm Structure of ABM Based AEKF

The common structure of an n th-order ECM is shown in Fig. 1. Generally, RC voltages and the SoC are combined together to form one augmented state vector, thus the state equation and output equation of the state-space model are expressed

as [22], [26]:

$$\begin{aligned} \begin{bmatrix} V_{RC_1,k+1} \\ \vdots \\ V_{RC_n,k+1} \\ SoC_{k+1} \end{bmatrix} &= \underbrace{\begin{bmatrix} e^{-\frac{T_s}{R_1 C_1}} & 0 & \cdots & 0 \\ 0 & \ddots & \ddots & \vdots \\ \vdots & \ddots & e^{-\frac{T_s}{R_n C_n}} & 0 \\ 0 & \cdots & 0 & 1 \end{bmatrix}}_{A_k} \begin{bmatrix} V_{RC_1,k} \\ \vdots \\ V_{RC_n,k} \\ SoC_k \end{bmatrix} \\ &+ \underbrace{\begin{bmatrix} R_1(1 - e^{-\frac{T_s}{R_1 C_1}}) \\ \vdots \\ R_n(1 - e^{-\frac{T_s}{R_n C_n}}) \\ \eta T_s / C_{cap} \end{bmatrix}}_{B_k} I_k, \quad (1) \\ \underbrace{V_t, k+1}_{y_{k+1}} &= \underbrace{\sum_{i=1}^n V_{RC_i, k+1} + OCV(SoC_{k+1})}_{g(x_{k+1}, u_{k+1})} + \underbrace{R_o}_{D_{k+1}} \underbrace{I_{k+1}}_{u_{k+1}}. \quad (2) \end{aligned}$$

where k denotes the time index, T_s denotes the sampling time interval, the positive current I_k represents charging, R_o represents the Ohmic resistance, V_{RC_i} represents the voltage across the corresponding RC network (consists of capacitance C_i and resistance R_i), V_t represents the battery terminal voltage, OCV is the function of SoC, η denotes the Coulombic efficiency, which is defined as the ratio between discharge and charge capacities, C_{cap} denotes the capacity of the battery, x_k is the state vector, y_k is the output vector, u_k is the input vector, $g(x_k, u_k)$ is a nonlinear measurement function, and A_k , B_k and D_k are system matrices of the state-space model.

TABLE I
OPERATION PROCESS OF ABM BASED AEKF ESTIMATION METHOD

Initialization ($k = 0$)	
Set \hat{x}_0^+ , P_0^+ , Q_0^+ , R_0^+	
Time update ($k = 1, 2, \dots$)	
Prior state:	$\hat{x}_k^- = A_{k-1} \hat{x}_{k-1}^+ + B_{k-1} u_{k-1}$ (3)
Prior error covariance:	$P_k^- = A_{k-1} P_{k-1}^+ A_{k-1}^T + \hat{Q}_{k-1}$ (4)
Innovation ¹ :	$e_k^- = y_k - C_k \hat{x}_k^- - D_k u_k$ (5)
Measurement update ($k = 1, 2, \dots$)	
Kalman gain matrix:	$K_k = P_k^- C_k^T / (C_k P_k^- C_k^T + \hat{R}_{k-1})$ (6)
Posterior state:	$\hat{x}_k^+ = \hat{x}_k^- + K_k e_k^-$ (7)
Posterior error covariance:	$P_k^+ = (I - K_k C_k) P_k^-$ (8)
Adaptive algorithm ($k = M, M+1, \dots$) ²	
Variance-covariance matrix:	$\hat{C}_v = (1/M) \sum_{i=k-M+1}^k e_i^- (e_i^-)^T$ (9)
Process noise covariance:	$\hat{Q}_k = K_k \hat{C}_v K_k^T$ (10)
Measurement noise covariance:	$\hat{R}_k = \hat{C}_v + C_k P_k^+ C_k^T$ (11)

¹ $C_k = \frac{\partial g(x_k, u_k)}{\partial x_k} \Big|_{x_k = x_k^-}$.

² M is the size of moving window.

Based on (1) and (2), the detailed operation process of ABM based AEKF estimation method is summarized in Table I [27].

B. Cross Interference in Kalman Gain

It can be derived from (1) that SoC is calculated through the CC method in the state equation. On the other hand, by the prior knowledge of RC voltages calculated from the state equation, SoC can also be derived through the OCV measurement method based on the OCV value obtained from the output equation. In the EKF related algorithm, the computation of K_k is the most critical part, because it determines whether the CC method or the OCV measurement method gives more weight to the final estimated SoC.

According to the properties of the covariance matrix, the detailed expression of P_k^- can be defined as [28]:

$$P_k^- = \left\{ p_{ij,k}^- \right\}_{(n+1) \times (n+1)}, p_{ij,k}^- = p_{ji,k}^-, i, j = 1, 2, \dots, n+1, \quad (12)$$

Specifically, the off-diagonal terms in the covariance matrix can be further expressed as [28]:

$$p_{ij,k}^- = \rho_{ij,k} \sqrt{p_{ii,k}^-} \sqrt{p_{jj,k}^-}, i, j = 1, 2, \dots, n+1 \& i \neq j \quad (13)$$

where $\rho_{ij,k}$ represents the correlation coefficient, which is the measurement of the linear dependence between $x_{i,k}$ and $x_{j,k}$, and $|\rho_{ij,k}| \leq 1$. Specifically, $\rho_{ij,k} > 0$ indicates the positive correlation, $\rho_{ij,k} < 0$ indicates the negative correlation and $\rho_{ij,k} = 0$ indicates no correlation.

It can be inferred from (13) that $p_{ij,k}^-$ contains the information of both $x_{i,k}$ and $x_{j,k}$. Thus, the off-diagonal terms in the covariance matrix represent the cross interference between the corresponding state variables.

Substituting (12) into (6), the detailed expression of K_k with respect to RC voltage ($K_{l,k}$, $l = 1, \dots, n$) and SoC ($K_{n+1,k}$) can be expressed as

$$\begin{bmatrix} K_{1,k} \\ \vdots \\ K_{n,k} \\ K_{n+1,k} \end{bmatrix} = \frac{1}{E} \begin{bmatrix} \sum_{j=1}^n p_{1j,k}^- + p_{1(n+1),k}^- & \frac{dOCV_k}{dSoC_k} \\ \vdots & \vdots \\ \sum_{j=1}^n p_{nj,k}^- + p_{n(n+1),k}^- & \frac{dOCV_k}{dSoC_k} \end{bmatrix} \quad (14)$$

$$K_{n+1,k} = \frac{1}{E} \left(\sum_{j=1}^n p_{(n+1)j,k}^- + p_{(n+1)(n+1),k}^- \frac{dOCV_k}{dSoC_k} \right) \quad (15)$$

where

$$E = \sum_{i=1}^n \sum_{j=1}^n p_{ij,k}^- + 2 \sum_{j=1}^n p_{(n+1)j,k}^- \frac{dOCV_k}{dSoC_k} + p_{(n+1)(n+1),k}^- \left(\frac{dOCV_k}{dSoC_k} \right)^2 + r_k \quad (16)$$

It can be obtained from (14) and (15) that besides the variances of RC voltages ($p_{ij,k}^-$, $i, j = 1, \dots, n$) and the vari-

ances of the SoC ($p_{(n+1)(n+1),k}^-$), the covariances of SoC and V_{RC_i} ($p_{(n+1)j,k}^-$, $j = 1, \dots, n$), which represent the cross interference terms between these two types of state variables, also have a great influence on the values of Kalman gain. Taking the convergence process as an example, when the adaptive algorithm is conducted, the elements of P_k converge to the steady state rapidly with various rates. Different changing ratios among variances and covariances lead to the fluctuation of the Kalman gain, which in turn causes the oscillation of estimation (SoC and V_{RC}).

However, there are no explicit correlations between RC voltages and SoC, which also means that the corresponding correlation coefficients ($\rho_{i(n+1),k}$, $i = 1, 2, \dots, n$) should be zero. Taking the charging scenario as an example, if the capacitors in the RC networks are not fully charged, the RC voltages and the SoC increase simultaneously when the charging current keeps constant or varies slightly, thus the positive correlation coefficients are obtained. After the capacitors are fully charged, the corresponding RC voltages maintain constant while the SoC still increases, thus the values of $\rho_{i(n+1),k}$ keep decreasing and approaching zero. Besides, considering a condition that the charging current suddenly drops to a low value, the decreasing tendency caused by the $e^{-\frac{T_s}{R_i C_i}} V_{R_i C_i, k}$ term accounts for a larger proportion, in comparison to the increasing tendency caused by the $R_i I_i (1 - e^{-\frac{T_s}{R_i C_i}})$ term. It can be seen from (1) that the overall RC voltages present decreasing tendencies. On the other hand, the SoC still increases due to the positive current. As a result, negative correlation coefficients are obtained in this condition. Similar results can be inferred in the discharging scenario. Hence, it can be concluded that there are no explicit correlations between RC voltages and SoC, thus the cross interference between them should be eliminated.

III. SBM BASED AEKF ESTIMATION METHOD

A. Structure of SBM

In order to decouple the relationship between the RC voltages and the SoC, the conventional ABM is split into two submodels: the RC voltage submodel and the SoC submodel. The discrete-time state-space functions of the two submodels are shown as

The RC voltage submodel [22], [26]:

$$\underbrace{\begin{bmatrix} V_{RC1,k+1} \\ \vdots \\ V_{RCn,k+1} \end{bmatrix}}_{x_{1,k+1}} = \underbrace{\begin{bmatrix} e^{-\frac{T_s}{R_1 C_1}} & \cdots & 0 \\ \vdots & \ddots & \vdots \\ 0 & \cdots & e^{-\frac{T_s}{R_n C_n}} \end{bmatrix}}_{A_{1,k}} \underbrace{\begin{bmatrix} V_{RC1,k} \\ \vdots \\ V_{RCn,k} \end{bmatrix}}_{u_{1,k}} + \underbrace{\begin{bmatrix} R_1(1 - e^{-\frac{T_s}{R_1 C_1}}) & 0 \\ \vdots & \vdots \\ R_n(1 - e^{-\frac{T_s}{R_n C_n}}) & 0 \end{bmatrix}}_{B_{1,k}} \underbrace{\begin{bmatrix} I_k \\ SoC_k \end{bmatrix}}_{u_{1,k}}^T \quad (17)$$

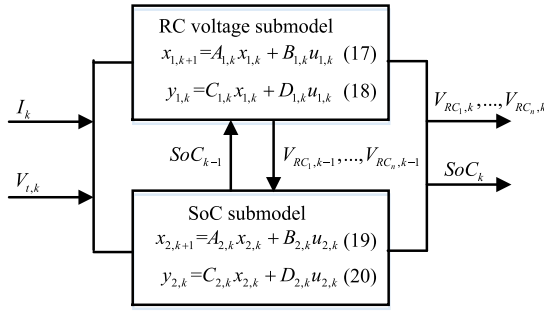


Fig. 2. Block diagram of split battery model.

$$\underbrace{V_{t,k}}_{y_{1,k}} = \underbrace{[1 \cdots 1]}_{C_{1,k}} [V_{RC1,k} \cdots V_{RCn,k}] + \underbrace{[R_o \ dOCV_k/dSoC_k]}_{D_{1,k}} [I_k \ SoC_k]^T \quad (18)$$

The SoC submodel [22], [26]:

$$\underbrace{SoC_{k+1}}_{x_{2,k+1}} = \underbrace{1}_{A_{2,k}} \cdot SoC_k + \underbrace{[\eta T_s / C_{cap} \ 0 \cdots 0]}_{B_{2,k}} \underbrace{[I_k \ V_{RC1,k} \cdots V_{RCn,k}]}_{u_{2,k}}^T \quad (19)$$

$$\underbrace{V_{t,k}}_{y_{2,k}} = \underbrace{(dOCV_k/dSoC_k)}_{C_{2,k}} SoC_k + \underbrace{[R_o \ 1 \cdots 1]}_{D_{2,k}} [I_k \ V_{RC1,k} \cdots V_{RCn,k}]^T \quad (20)$$

where $x_{1,k}$, $y_{1,k}$ and $u_{1,k}$ are the state vector, output vector and input vector of the RC voltage submodel, $A_{1,k}$, $B_{1,k}$, $C_{1,k}$ and $D_{1,k}$ are system matrices of the RC voltage submodel. Similarly, $x_{2,k}$, $y_{2,k}$ and $u_{2,k}$ are the state vector, output vector and input vector of the SoC submodel, $A_{2,k}$, $B_{2,k}$, $C_{2,k}$ and $D_{2,k}$ are system matrices of the SoC submodel.

It can be concluded from (17)–(20) that the augmented state vector in (1) is divided into two parts: the vector only contains RC voltages, and the vector only contains the SoC. Equation (17) indicates that the state variable of the SoC submodel is involved in the input vector of the RC voltage submodel. Similarly, the input vector of the SoC submodel contains state variables of the RC voltage submodel, as illustrated in (19). Hence, the complete model is formed by combining the two submodels together, as shown in Fig. 2.

B. Discussion of Kalman Gain

Based on (6), the detailed expressions of the Kalman gain with respect to the RC voltage submodel and SoC submodel are

shown as

$$\begin{bmatrix} K_{11,k} \\ \vdots \\ K_{1n,k} \end{bmatrix} = \frac{1}{\sum_{i=1}^n \sum_{j=1}^n p_{ij,k}^- + r_{1,k}} \begin{bmatrix} \sum_{j=1}^n p_{1j,k}^- \\ \vdots \\ \sum_{j=1}^n p_{nj,k}^- \end{bmatrix} \quad (21)$$

$$K_{2,k} = \frac{p_{2,k}^- \frac{dOCV_k}{dSoC_k}}{p_{2,k}^- \left(\frac{dOCV_k}{dSoC_k} \right)^2 + r_{2,k}} \quad (22)$$

where $r_{1,k}$ and $r_{2,k}$ denote the measurement covariances for the RC voltage submodel and the SoC submodel, respectively.

It can be observed from (21) that $K_{1,k}$ is only related to the covariances among RC voltages ($p_{ij,k}^-$, $i, j = 1, \dots, n$) and the measurement covariance ($r_{1,k}$). Meanwhile, it can be noted from (22) that $K_{2,k}$ is mainly affected by three factors: the variance of SoC ($p_{2,k}^-$), the measurement covariance ($r_{2,k}$) and the OCV changing rate with respect to SoC ($dOCV_k/dSoC_k$). Hence, it can be concluded that the cross interference terms between RC voltages and SoC are eliminated in (21) and (22). In addition, both of expressions have been simplified, in comparison to (14) and (15).

It can be concluded from (22) that the value of $dOCV_k/dSoC_k$ has a significant influence on $K_{2,k}$. For some types of battery chemistries, such as the LiFePO₄ battery, the SoC-OCV curve is quite flat during a wide SoC range, which means that the value of $dOCV_k/dSoC_k$ is almost zero in this region, and SoC is a quasi-unobservable state variable for the OCV measurement method. In this case, if the estimated value of $r_{2,k}$ is also too small, a relatively large value of $K_{2,k}$ is obtained. On one hand, this would lead to the divergence of the system. On the other hand, the OCV measurement method, which leads to a large estimation error, gives more weight to the final estimated SoC. Hence, the lower limit of $r_{2,k}$ ($r_{2,k,lim}$) needs to be set in an appropriate range to ensure the stability and fidelity of the estimation, especially for batteries with a wide range of flat SoC-OCV curve.

C. Algorithm Framework

In this paper, the RC voltage estimation and the SoC estimation are executed based on a decoupled SBM. Since for the electrical vehicle applications, the SoC is more concerned by designers and consumers when compared to RC voltages, thus the adaptive algorithm is only applied to the SoC estimation, which can also reduce the computation cost of the algorithm. In most working scenarios, SoC changes gradually during a short time interval, thus the OCV value and impedance parameters, which present progressive variations with SoC and are essential for the RC voltage estimation, can be considered as constant during the specific time interval. Hence, the estimation algorithm based on the RC voltage submodel can be firstly implemented with the SoC value estimated from the last time index. After that, the SoC submodel updates RC voltages estimated from the first estimation algorithm to accurately estimate the SoC, and then, the estimated value is provided back to the RC voltage submodel. The block diagram of the proposed estimation method is shown in Fig. 3.

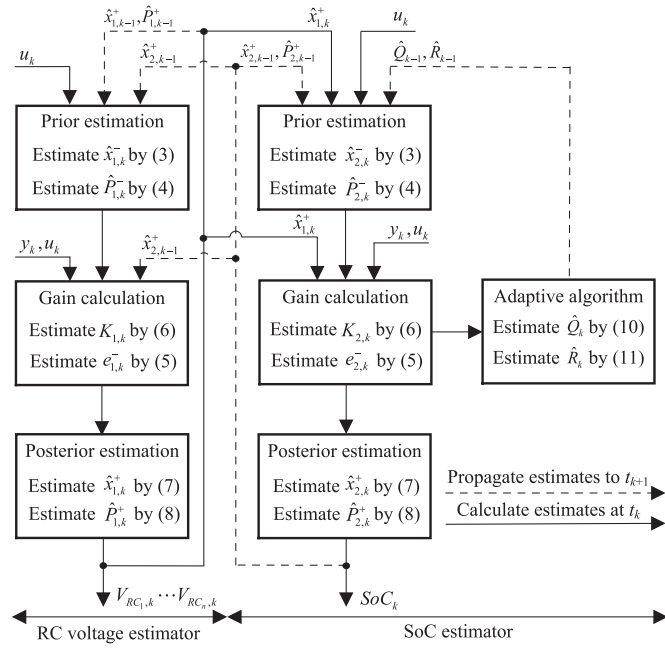


Fig. 3. Block diagram of proposed estimation method.

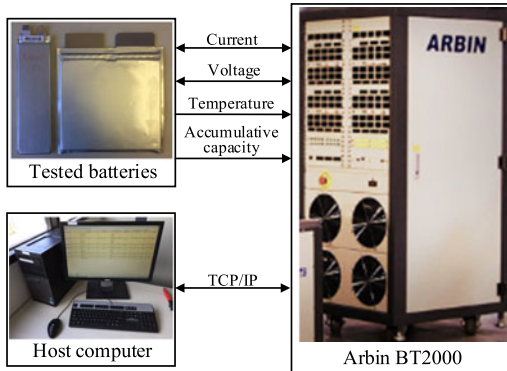


Fig. 4. The structure of the test platform.

 TABLE II
 SPECIFICATIONS FOR TEST BATTERIES

Battery chemistry	LiFePO ₄	LiNMC
Nominal capacity	10.50 Ah	40 Ah
Nominal voltage	3.2 V	3.7 V
Charge cutoff voltage	3.65 V	4.2 V
Discharge cutoff voltage	2.0 V	2.7 V

IV. EXPERIMENTAL TESTS

A. Experimental Setup

As shown in Fig. 4, a test platform is established to verify the effectiveness of the proposed method. The test platform consists of the tested batteries, an Arbin BT2000 battery cycler, and a host computer to program and store experimental data. Two categories of lithium-ion cell chemistries, i.e., the LiFePO₄ and the LiNMC batteries, are selected for the test. The specifications for tested batteries are presented in Table II. The 8-channel

 TABLE III
 PROCEDURE OF BATTERY CHARACTERIZATION TESTS

Step	Procedure
1.	Capacity test
2.	Charge/discharge SoC-OCV test
3.	Discharge hybrid pulse test
4.	Consecutive UDDS test

 TABLE IV
 CAPACITY TEST RESULTS

Battery chemistry	LiFePO ₄	LiNMC
Charge capacity	10.50 Ah	40.99 Ah
Discharge capacity	10.47 Ah	40.89 Ah
Columbic efficiency	99.71%	99.76%

Arbin BT2000 battery cycler is used to load current or power profiles on the tested batteries. Current and voltage sensors of each channel have accuracies of $\pm 0.02\%$ for low power and $\pm 0.05\%$ for high power applications. The measurement current and voltage ranges are $\pm 100\text{A}$ and $0\sim 5\text{ V}$, respectively. All of the tests are conducted at room temperature ($25 \pm 2^\circ\text{C}$). Data points, including current, voltage, temperature and accumulative capacity, are collected with the sampling rate of 1 Hz. Since the error of the current sensor in the battery cycler is less than 0.05%, and the initial conditions can be obtained precisely from the test platform, it is feasible to assume that the CC calculation results based on the recorded current can be considered as a reference value for comparison.

B. Battery Characterization Test Procedure

It can be inferred from (17) to (20) that the system matrices of the SBM contain one SoC-OCV relationship and a series of impedance parameters (R_o , R_i and C_i), which need to be identified firstly. In this paper, the battery model parameters are identified off-line through battery characterization tests. The detailed test procedure is presented in Table III.

The capacity test is composed of three charge/discharge cycles. In each cycle, the battery is charged using the constant-current constant-voltage method with the manufacture's recommended voltage and current. After that, the 0.5C constant-current discharge process is implemented until the discharge cutoff voltage is reached. A 60-minute rest period is conducted after each charge/discharge process. The charge/discharge capacity, which is calculated as the mean value of three cycles, will be applied for SoC calculations. The capacity test results, including the charge/discharge capacities and the Columbic efficiencies are presented in Table IV.

The charge/discharge SoC-OCV curves are extracted at 5% SoC interval with a 0.5C charge/discharge followed by a certain length of rest period (5-hour for the LiFePO₄ battery and 2-hour for the LiNMC battery). Considering the characteristic of nonlinearity, the polynomial function as shown in (23) is adopted to describe the average SoC-OCV relationship, as shown in

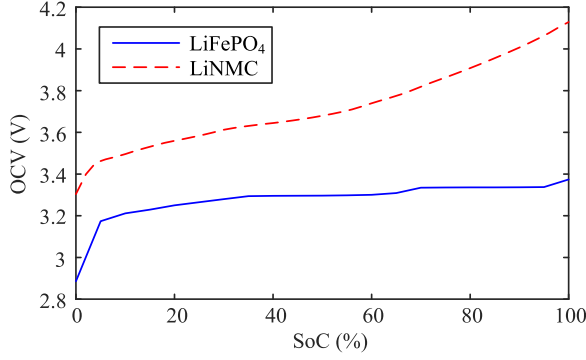


Fig. 5. SoC-OCV curve of two tested batteries.

Fig. 5.

$$V_{oc}(SoC) = \sum_{i=0}^{n_i} a_i SoC^i \quad (23)$$

where a_i is the polynomial coefficient which is extracted with the curve-fitting method, n_i is the order of the polynomial function. Compared with the LiNMC battery, the SoC-OCV relationship of the LiFePO₄ battery owns a stronger nonlinear characteristic, as shown in Fig. 5. Hence, n_i is set as 10 for the LiFePO₄ battery and 8 for the LiNMC battery. The specific values of a_i for the two batteries are listed as

LiFePO₄:

$$a_0 = 2.8862; a_1 = 11.064; a_2 = -154.23; a_3 = 1164.7; \\ a_4 = -5212.4; a_5 = 14744; a_6 = -27172; a_7 = 32603; a_8 = -24556; a_9 = 10531; a_{10} = -1959.1.$$

LiNMC:

$$a_0 = 3.3504; a_1 = 3.3149; a_2 = -31.783; a_3 = 189.42; \\ a_4 = -631.24; a_5 = 1200.9; a_6 = -1292.6; a_7 = 732.92; a_8 = -170.15.$$

To extract the impedance parameters, the discharge hybrid pulse test is conducted over the whole SoC range in steps of 5% SoC interval. In each interval, the test profile consists of five pairs of 20-second discharge and charge pulses (0.5C, 1.0C, 1.5C, 2.0C and 2.5C). Each discharge pulse is followed by a 40-second rest period, and each charge pulse is followed by a 60-second rest period. After the hybrid pulses, a 5% SoC decrease is realized by 0.5C discharge current, followed by a 2-hour rest. Impedance parameters of each SoC interval are identified through the least squares method.

Finally, the Urban Dynamometer Driving Schedule (UDDS) cycles with 10-minute rest periods are employed consecutively to prove the validity and advantages of the proposed method. The test begins by a known initial SoC value of 80%, thus the reference trajectory of SoC can be computed through the CC estimation method. The test is terminated when SoC drops below 20%. The current profile of UDDS is scaled such that the maximum discharge current is 2.5C and the maximum charge current is 2C.

V. EXPERIMENTAL VERIFICATION AND DISCUSSION

Based on the above analysis, the proposed estimation method can be applied to an ECM with any order. Considering a trade-

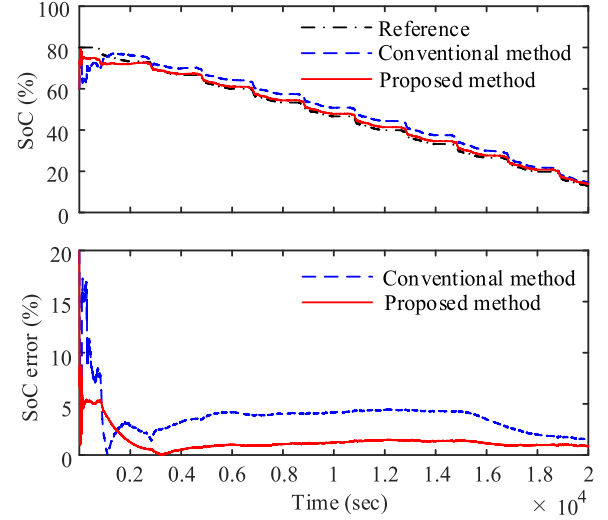


Fig. 6. Comparison of SoC estimation by two methods for LiFePO₄ battery.

off between the fidelity and the computational complexity, the second-order ECM is selected in this paper. To test the robustness of the proposed algorithm against the uncertain initialization and noise effects, the estimated SoC is erroneously initialized as 60%, and two random white noise is superimposed over the measured current and voltage datasets (the LiFePO₄ battery: $\sigma_I = 1$ A, $\sigma_V = 5$ mV; the LiNMC battery: $\sigma_I = 4$ A, $\sigma_V = 5$ mV).

A. Discussion of Estimation Results

To verify the advantages of the proposed SBM based AEKF method, the ABM based AEKF method, as one of the widely used techniques in the SoC estimation, is also conducted to make a comparison. The size of moving window is set as 100 throughout this paper, which also means that the adaptive algorithm is executed after 100 s.

1) *LiFePO₄ Battery:* It can be observed from Fig. 5 that two obvious plateaus exist in the SoC-OCV curve (during 35%–65% SoC and 70%–95% SoC, respectively). Based on the analysis in Section III, the value of $r_{2,k,\text{lim}}$ should be set as a relatively large value (comparing to the LiNMC battery) to ensure the stability and fidelity of the estimation. The value of $r_{2,k,\text{lim}}$ is set as 1×10^{-2} in this paper, and the results of SoC estimation by the conventional and the proposed methods are plotted in Fig. 6.

It can be observed from Fig. 6 that the evolution of the estimated SoC can be divided into two stages: the start-up stage and the stable stage.

The close look of the Kalman gain with respect to SoC and the SoC variation during the start-up stage is plotted in Fig. 7(a) and Fig. 7(b), respectively. It can be observed that the Kalman gain calculated by the conventional method exhibits obvious oscillation after the adaptive algorithm is executed (around 110 s), which in turn leads to the undesired oscillation of the estimated SoC, whose the largest error reaches 16.9%, as shown in Fig. 7(c). In addition, it can be noticed from Fig. 7(d) that the estimated RC voltages also fluctuate dramatically around

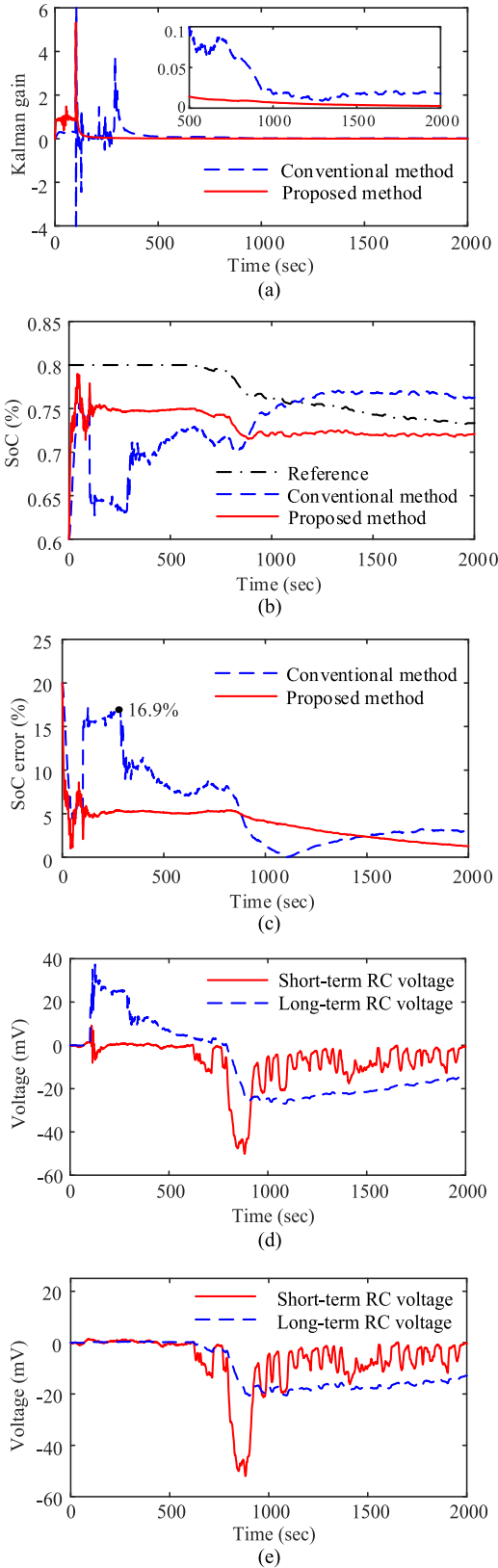


Fig. 7. Close look of estimation results during start-up stage. (a) Kalman gain with respect to SoC. (b) Estimated SoC. (c) SoC error. (d) Estimated RC voltages from the conventional method. (e) Estimated RC voltages from the proposed method.

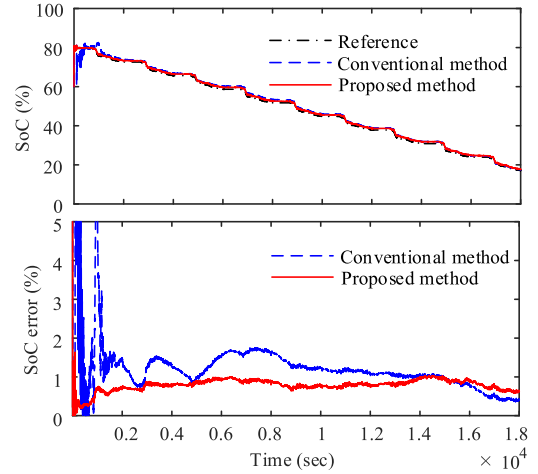


Fig. 8. Comparison of SoC estimation by two methods for LiNMC battery.

110 s. Because of correlations between RC voltages and SoC, the oscillation in the RC voltage estimation results in the oscillating OCV estimation, which in turn influences the estimated SoC. Hence, it can be concluded that the cross interference between RC voltages and SoC leads to the undesired oscillation in estimation and degrades the convergence performance.

In terms of the stable stage, the SoC error estimated by the conventional method reaches to 5% for a long period of time, which is caused by two reasons. On one hand, the cross interference between SoC and RC voltages reduce the estimation accuracy. The estimation error on RC voltages can result in the estimation error on the OCV, which in turn degrades the accuracy of the estimated SoC. On the other hand, according to (15), the lower value of $dOCV_k/dSoC_k$ during the plateau leads to a larger value of Kalman gain. It means that the OCV measurement method gives more weight to the final estimated SoC, in comparison with the CC method. Unfortunately, a large SoC error exists by the OCV measurement method due to the invertible characteristic of the flat SoC-OCV relationship, which can reduce the final SoC estimation accuracy.

By comparison, it can be observed from Fig. 6 that the result of SoC estimation by the proposed method converges to the reference value much smoother during the start-up stage. During the stable stage, the maximum SoC error is no more than 1%. As can be seen from Fig. 7, the Kalman gain converges to the stable value smoothly after the adaptive algorithm is adopted, and the undesired oscillations are eliminated in both the estimated SoC and RC voltages. The improvements are brought by the cross interference reduction, as a result of decoupling the SoC estimation and RC voltage estimation.

2) *LiNMC Battery*: Both the proposed and the conventional methods are applied on the experimental data of the LiNMC battery. Since the SoC-OCV curve of the LiNMC battery doesn't exist the obvious plateau, the restriction on the $r_{2,k,limit}$ is not very strict, and it is set as 1×10^{-4} in this paper. The estimation results are plotted in Figs. 8 and 9, which are similar to the results from the LiFePO₄ battery. It can be noted from Fig. 9 that at the start-up stage, the Kalman gain calculated by the

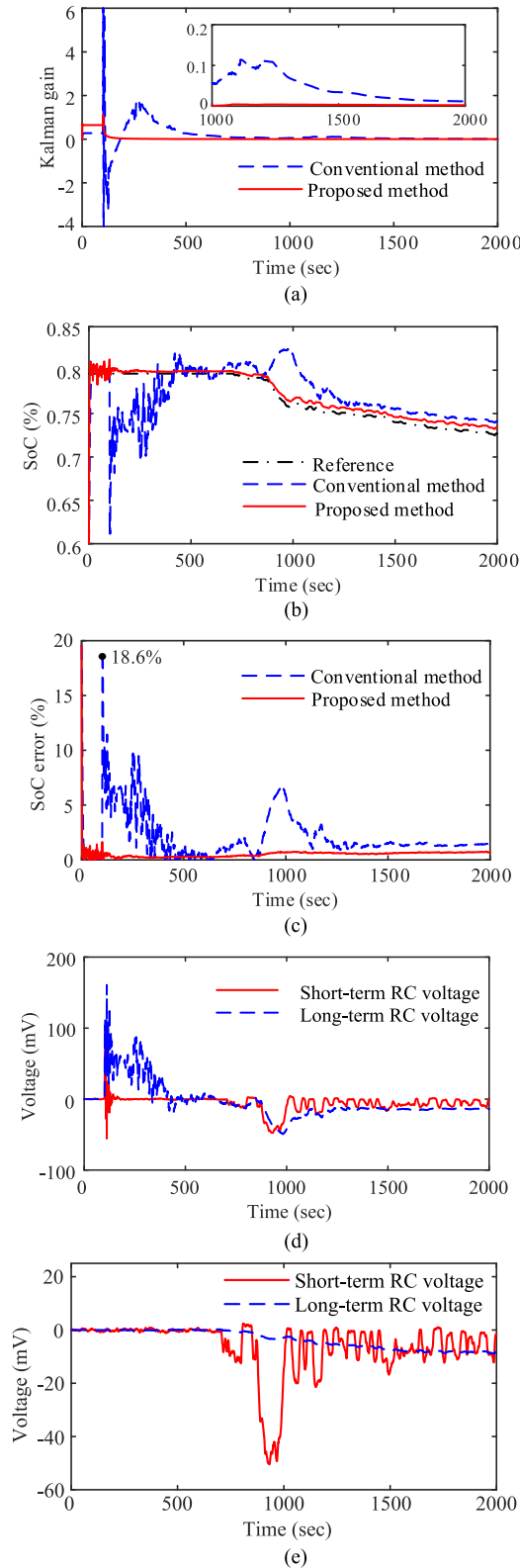


Fig. 9. Close look of estimation results during start-up stage. (a) Kalman gain with respect to SoC. (b) Estimated SoC. (c) SoC error. (d) Estimated RC voltages from the conventional method. (e) Estimated RC voltages from the proposed method.

TABLE V
COMPUTATIONAL TIME OF STATE ESTIMATION IN UDDS FOR
DIFFERENT BATTERIES

	Conventional method		Proposed method	
	LiFePO ₄	LiNMC	LiFePO ₄	LiNMC
Computational time	959 <i>us</i>	874 <i>us</i>	798 <i>us</i>	784 <i>us</i>

conventional method fluctuates dramatically at round 110 s, resulting in an undesired oscillation in the estimated SoC and RC voltages, and the maximum SoC error reaches 18.6%. In comparison, the proposed method eliminates the oscillation at the start-up stage and generates less error at the stable stage, which clearly indicates the advantage of the proposed method. Compared with the results from the LiFePO₄ battery, the results from the LiNMC battery show faster convergence speed and less steady state error, due to the steeper SoC-OCV curve.

B. Computational Cost

In the electric vehicle applications, the state estimation process needs to be implemented on-board through the embedded microcontrollers with limited calculation, storage and power resources. For that reason, it is worthwhile to investigate the computational cost of the proposed estimation method. In order to quantify the computational cost, each algorithm is implemented (on a 2.5-GHz processor and with 12-GB RAM) repeatedly for 10 times to obtain the average computational time of each time interval. The comparative results are shown in Table V. Due to the reduction of the matrix dimension, the proposed method reduces the computational time while improves the estimation performance at the same time. Since the average computational time for both categories of batteries is far less than 1 s, it is verified that the proposed method is eligible for on-board BMS applications, in which the sampling ratio is often set as less than 1 Hz.

VI. CONCLUSION

This paper presents a SBM based adaptive SoC estimation method. The proposed SBM is achieved by dividing the conventional ABM into two parts: the RC voltage submodel and the SoC submodel. The model partition helps reduce the cross interference between the RC voltages and the SoC. Thus, the oscillation in the states estimation is degraded at the start-up stage, and the estimation accuracy is improved during the stable stage. Two types of lithium-ion batteries, including the LiFePO₄ battery and the LiNMC battery, are employed under test, and a case of a second-order ECM is analyzed. Comparative results show that the proposed method demonstrates a higher stability during the start-up stage and constrains the SoC error within 1% during the stable stage, regardless of the incorrect initial SoC and additional sensor noise. Moreover, the average computational time of the proposed method is far less than 1 s, which verifies its feasibility in on-board applications.

In this paper, all of the model parameters are identified off-line and considered as univariate functions of SoC. However,

model parameters, such as the impedance parameters and the charge/discharge capacities, are also influenced by many other factors in the electric vehicle applications, such as the C-rate of load current, the temperature and aging levels. Therefore, the future work will be concentrated on the integration of the SBM based adaptive SoC estimation method to the on-line parameter identification, which can update model parameters in real time to further improve the accuracy of SoC estimation.

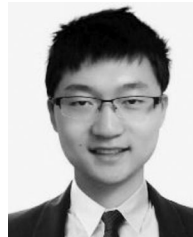
REFERENCES

- [1] X. Zhang and C. Mi, *Vehicle Power Management: Modeling, Control and Optimization*. Berlin, Germany: Springer, 2011.
- [2] L. Lu, X. Han, J. Li, J. Hua, and M. Ouyang, "A review on the key issues for Lithium-ion battery management in electric vehicles," *J. Power Sources*, vol. 226, pp. 272–288, 2013.
- [3] Y. Shang, B. Xia, F. Lu, C. Zhang, N. Cui, and C. Mi, "A switched-coupling-capacitor equalizer for series-connected battery strings," *IEEE Trans. Power Electron.*, vol. 32, no. 10, pp. 7694–7706, Oct. 2017.
- [4] B. Xia, T. Nguyen, J. Yang, and C. Mi, "The improved interleaved voltage measurement method for series connected battery packs," *J. Power Sources*, vol. 334, pp. 12–22, 2016.
- [5] B. Xia, Y. Shang, T. Nguyen, and C. Mi, "A correlation based fault detection method for short circuits in battery packs," *J. Power Sources*, vol. 337, pp. 1–10, 2017.
- [6] M. Petzl and M. A. Danzer, "Advancements in OCV measurement and analysis for Lithium-ion batteries," *IEEE Trans. Energy Convers.*, vol. 28, no. 3, pp. 675–681, Sep. 2013.
- [7] H. He, X. Zhang, R. Xiong, Y. Xu, and H. Guo, "Online model-based estimation of state-of-charge and open-circuit voltage of Lithium-ion batteries in electric vehicles," *Energy*, vol. 39, pp. 310–318, 2012.
- [8] P. Singh, C. Fennie Jr., and D. Reisner, "Fuzzy logic modelling of state-of-charge and available capacity of Nickel/metal hydride batteries," *J. Power Sources*, vol. 136, pp. 322–333, Oct. 1, 2004.
- [9] Y. L. Murphey *et al.*, "Intelligent hybrid vehicle power control—Part II: Online intelligent energy management," *IEEE Trans. Veh. Technol.*, vol. 62, no. 1, pp. 69–79, Jan. 2013.
- [10] M. Charkhgard and M. Farrokhi, "State-of-charge estimation for Lithium-ion batteries using neural networks and EKF," *IEEE Trans. Ind. Electron.*, vol. 57, no. 12, pp. 4178–4187, Dec. 2010.
- [11] Q.-S. Shi, C.-H. Zhang, and N.-X. Cui, "Estimation of battery state-of-charge using ν -support vector regression algorithm," *Int. J. Automot. Technol.*, vol. 9, pp. 759–764, 2008.
- [12] Z. Chen, Y. Fu, and C. C. Mi, "State of charge estimation of Lithium-ion batteries in electric drive vehicles using extended Kalman filtering," *IEEE Trans. Veh. Technol.*, vol. 62, no. 3 pp. 1020–1030, Mar. 2013.
- [13] Z. Chen, B. Xia, and C. C. Mi, "A novel state-of-charge estimation method for Lithium-ion battery pack of electric vehicles," in *Proc. 2015 IEEE Transp. Electrification Conf. Expo*, 2015, pp. 1–6.
- [14] Y. Zhang, R. Xiong, and H. He, "Evaluation of the model-based state-of-charge estimation methods for Lithium-ion batteries," in *Proc. 2016 IEEE Transp. Electrification Conf. Expo*, 2016, pp. 1–8.
- [15] Y. Wang, C. Zhang, and Z. Chen, "A method for state-of-charge estimation of LiFePO₄ batteries at dynamic currents and temperatures using particle filter," *J. Power Sources*, vol. 279, pp. 306–311, 2015.
- [16] C. Lin, H. Mu, R. Xiong, and W. Shen, "A novel multi-model probability battery state of charge estimation approach for electric vehicles using H-infinity algorithm," *Appl. Energy*, vol. 166, pp. 76–83, Mar. 15, 2016.
- [17] F. Zhang, G. Liu, L. Fang, and H. Wang, "Estimation of battery state of charge with H_∞ observer: Applied to a robot for inspecting power transmission lines," *IEEE Trans. Ind. Electron.*, vol. 59, no. 2, pp. 1086–1095, Feb. 2012.
- [18] J. Xu, B. Cao, J. Cao, Z. Zou, C. C. Mi, and Z. Chen, "A comparison study of the model based SOC estimation methods for Lithium-ion batteries," in *Proc. 2013 IEEE Veh. Power Propulsion Conf.*, 2013, pp. 1–5.
- [19] X. Chen, W. Shen, Z. Cao, and A. Kapoor, "A novel approach for state of charge estimation based on adaptive switching gain sliding mode observer in electric vehicles," *J. Power Sources*, vol. 246, pp. 667–678, 2014.
- [20] J. Lee, O. Nam, and B. Cho, "Li-ion battery SOC estimation method based on the reduced order extended Kalman filtering," *J. Power Sources*, vol. 174, pp. 9–15, 2007.
- [21] H. He, R. Xiong, X. Zhang, F. Sun, and J. Fan, "State-of-charge estimation of the Lithium-ion battery using an adaptive extended Kalman filter based on an improved Thevenin model," *IEEE Trans. Veh. Technol.*, vol. 60, no. 4, pp. 1461–1469, May 2011.
- [22] F. Sun, R. Xiong, and H. He, "A systematic state-of-charge estimation framework for multi-cell battery pack in electric vehicles using bias correction technique," *Appl. Energy*, vol. 162, pp. 1399–1409, 2016.
- [23] R. Xiong, F. Sun, X. Gong, and C. Gao, "A data-driven based adaptive state of charge estimator of Lithium-ion polymer battery used in electric vehicles," *Appl. Energy*, vol. 113, pp. 1421–1433, 2014.
- [24] C. Zhang, L. Y. Wang, X. Li, W. Chen, G. G. Yin, and J. Jiang, "Robust and adaptive estimation of state of charge for Lithium-ion batteries," *IEEE Trans. Ind. Electron.*, vol. 62, no. 8, pp. 4948–4957, Aug. 2015.
- [25] Z. L. Zhang, X. Cheng, Z. Y. Lu, and D. J. Gu, "SOC estimation of Lithium-ion batteries with AEKF and wavelet transform matrix," *IEEE Trans. Power Electron.*, vol. 32, no. 10, pp. 7626–7634, Oct. 2017.
- [26] J. Yang, B. Xia, Y. Shang, W. Huang, and C. Mi, "Improved battery parameter estimation method considering operating scenarios for HEV/EV applications," *Energies*, vol. 10, pp. 1–20, 2016.
- [27] R. Xiong, H. He, F. Sun, and K. Zhao, "Evaluation on state of charge estimation of batteries with adaptive extended Kalman filter by experiment approach," *IEEE Trans. Veh. Technol.*, vol. 62, no. 1, pp. 108–117, Jan. 2013.
- [28] J. Rice, *Mathematical Statistics and Data Analysis*. Scarborough, ON, Canada: Nelson Education, 2006.



Jufeng Yang (S'15) received the B.S. degree in electrical engineering in 2012 from Nanjing University of Aeronautics and Astronautics, Nanjing, China, where he is currently working toward the Ph.D. degree (Master-Doctorate program) in electrical engineering. In 2015, he received the funding from China Scholarship Council, and became a joint Ph.D. student in the Department of Electrical and Computer Engineering, San Diego State University, San Diego, CA, USA.

His research interests focus on battery management systems, including battery modeling, battery model parameter identification, and battery state estimation.



Bing Xia (S'13) received the B.S. degree in mechanical engineering from the University of Michigan, Ann Arbor, MI, USA, and the B.S. degree in electrical engineering from Shanghai Jiaotong University, Shanghai, China, in 2012. He was a Ph.D. student in automotive system engineering at the University of Michigan Dearborn between winter 2013 and summer 2015. Since Fall 2015, he has been a Ph.D. candidate in the joint Ph.D. program with San Diego State University, San Diego, CA, USA, and the University of California, San Diego, CA, USA.

His research interests focus on batteries, including charging optimization, battery safety, and battery management.



Yunlong Shang (S'14) received the B.S. degree in automation from Hefei University of Technology, Hefei, China, in 2008. Since 2010, he has been working toward the Ph.D. degree in the School of Control Science and Engineering, Shandong University, Shandong, China. In 2015, he received the funding from China Scholarship Council, and became a joint Ph.D. student in the Department of Electrical and Computer Engineering, San Diego State University, San Diego, CA, USA.

His current research interests include the design and control of battery management systems and battery equalizers, battery modeling, and battery state estimation.



Wenxin Huang (M'09) received the B.S. degree in the Southeast University, Nanjing, China, in 1988, and the M.S. and Ph.D. degrees from Nanjing University of Aeronautics and Astronautics (NUAA), Nanjing, China, in 1994 and 2002, respectively.

In 2003, he joined the faculty of the College of Automation Engineering, NUAA, where he is currently a Professor. His research interests include stand-alone power systems, design and control for electrical machine systems, power electronics, renewable energy generating systems, and battery management

systems.



Chunting Chris Mi (S'00–A'01–M'01–SM'03–F'12) received the B.S.E.E. and M.S.E.E. degrees in electrical engineering from Northwestern Polytechnical University, Xi'an, China, in 1985 and 1988, respectively. He received the Ph.D. degree in electrical engineering from the University of Toronto, Toronto, ON, Canada, in 2001.

He is currently a Professor and the Chair of electrical and computer engineering and the Director of the Department of Energy—funded Graduate Automotive Technology Education Center for Electric Drive Transportation, San Diego State University, San Diego, USA. Prior to joining SDSU, he was with the University of Michigan, Dearborn, MI, USA, from 2001 to 2015.

He has conducted extensive research and has published more than 100 journal papers. His research interests include electric drives, power electronics, electric machines, renewable-energy systems, and electrical and hybrid vehicles.